University of Kent

Kent Academic Repository

Ghrabat, Fadhil, Zhu, Huiling and Wang, Jiangzhou (2024) ***Machine learning-based intelligent localization technique for channel classification in massive MIMO.*** **Discover Internet of Things, 4 .**

Downloaded from

https://kar.kent.ac.uk/107593/ The University of Kent's Academic Repository KAR

The version of record is available from

https://doi.org/10.1007/s43926-024-00070-9

This document version

Publisher pdf

DOI for this version

Licence for this version

CC BY-NC-ND (Attribution-NonCommercial-NoDerivatives)

Additional information

Versions of research works

Versions of Record

If this version is the version of record, it is the same as the published version available on the publisher's web site. Cite as the published version.

Author Accepted Manuscripts

If this document is identified as the Author Accepted Manuscript it is the version after peer review but before type setting, copy editing or publisher branding. Cite as Surname, Initial. (Year) 'Title of article'. To be published in ***Title of Journal*** , Volume and issue numbers [peer-reviewed accepted version]. Available at: DOI or URL (Accessed: date).

Enquiries

If you have questions about this document contact ResearchSupport@kent.ac.uk. Please include the URL of the record in KAR. If you believe that your, or a third party's rights have been compromised through this document please see our Take Down policy (available from https://www.kent.ac.uk/guides/kar-the-kent-academic-repository#policies).

Discover Internet of Things

Research

Machine learning-based intelligent localization technique for channel classification in massive MIMO

Fadhil Ghrabat[1,2] · **Huiling Zhu**[1] · **Jiangzhou Wang**[1]

Received: 2 February 2024 / Accepted: 9 September 2024
Published online: 22 October 2024
© The Author(s) 2024 OPEN

Abstract
Multiple-input multiple-output (MIMO) technology has been widely adopted in wireless communications, which enables the simultaneous transmission of multiple data streams via multiple transmitting and receiving antennas. In a MIMO system with non-line-of-sight (NLOS), transmitted signals are reflected by various obstacles along the path, reaching the antenna at different angles and times. In 5G networks, the NLOS problem is a major challenge for massive MIMO localization, significantly reducing positioning accuracy. In this work, an intelligent localization technique based on NLOS identification and mitigation is proposed to address this problem. In this solution, a Convolutional Neural Network (CNN) based hybrid Archimedes-based Salp Swarm Algorithm (HASSA) technique is proposed to detect NLOS or the line of sight (LOS) and estimate the location. The accuracy can be analyzed by considering the angle of arrival of signals, threshold-based time of arrival, and time difference of arrival from different antennas. A novel reinforcement learning-based optimization approach is used for the mitigation of NLOS in the radio wave propagation path, which in turn reduces the computational complexity. We use the Ensemble Deep Deterministic Policy Gradient-Based Approach (EDDPG)-based Honey Badger algorithm (HBA) for the aforementioned process. The simulation of this approach assesses diverse scenarios and considers different parameters, and the approach is compared with various state-of-the-art works. From the simulation results, our proposed approach can be used for the identification and detection of LOS and NLOS components and can precisely enhance the localization compared with other approaches.

Article Highlights

- The study uncovers key channel features essential for effectively managing NLOS conditions.
- The proposed CNN-based method improves location accuracy in 5G by effectively distinguishing between LOS and NLOS conditions.
- The novel algorithm improves 5G localization by reducing NLOS errors, offering high accuracy with minimal computational overhead.

Keywords Line of sight (LOS) · Non line of sight (NLOS) · Massive MIMO · CNN · Salp swarm algorithm (SSA) · EDDPG · CIR · Identification and mitigation

✉ Fadhil Ghrabat, fg240@kent.ac.uk; fadel@utq.edu.iq; Huiling Zhu, h.zhu@kent.ac.uk; Jiangzhou Wang, j.z.wang@kent.ac.uk | [1]School of Engineering, University of Kent, Canterbury CT2 7NT, UK. [2]College of Engineering, University of Thi-Qar, Nasiriyah, Thi-Qar, 64001, Iraq.

1 Introduction

Over the past 20 years, localization strategies have gained significant attention with the rise of personal electronic devices and commercial wireless networks. 5G networks offer high accuracy owing to disruptive technologies like millimeter-wave communication, and massive multiple-input-multiple-output (MIMO) antennas. Massive MIMO enhances channel resolution and reduces interference, enabling fast communications in 5G networks. However, in 5G massive MIMO networks with a large number of antennas at the transmitter and receiver, the non-line-of-sight (NLOS) problem is the main challenge for localization, which seriously reduces the positioning accuracy [1]. Different obstacles in the path distract the transmitted signals, causing them to reach the antenna at different angles and times and resulting in signal reflections and multipath propagation [2]. Localization techniques frequently utilize variables such as time of arrival (TOA), angle of arrival (AOA), angle of departure (AOD), and received signal strength. The multipath and scattering environment greatly influence the NLOS error, which in turn affects TOA, AOA, and AOD. Appropriately identifying the type of channel environment enables the elimination of errors caused by the NLOS environment and increases the precision and accuracy of localization, thereby improving the overall reliablity of the communication system [3, 4].

The channel identification assisted localization-based method involves a two-step procedure: NLOS identification followed by position estimation. The characteristics of the received signal are analyzed to identify the line-of-sight (LOS) path [5]. The channel is then classified as NLOS or LOS. Numerous proposals have been presented for studies on identifying the LOS/NLOS channel for localization [6, 7]. For instance, in [8] machine learning techniques are adopted to identify LOS and NLOS in vehicle-to-vehicle networks. The power angular spectrum is an estimated high-resolution parameter for identifying objects from multipath components (MPCs). Measurement data were collected from various features to determine their feasibility. The technique incorporated and applied multiple features. It was compared with previous methods of training. This technique was robust, accurate, and feasible. However, it was a complicated one when the application required considerable signals to be analyzed. Furthermore, the mitigation process is also not mentioned. To analyze the Fisher information, Mendrzik et al. [9] presented a 5G millimeter-wave MIMO system to position NLOS components. An equivalent Fisher information matrix (EFIM) was derived from a large number of antennas to transmit and receive data over a large bandwidth. The direction and location decreased the position error bound and orientation error bound for each part of NLOS. The evaluated position and orientation were feasible, and the accuracy increased. Nonetheless, the computational complexity was higher than that of other approaches. Jian et al. [10] proposed an orbital angular momentum (OAM)-MIMO transmission system. The radius was different for multiple uniform circular arrays with the same center. The preprocessing scheme was determined by OAM modes for singular value decomposition. The coding operations of various modes were superior to those of the conventional MIMO. The demand for transmitting and receiving data in an NLOS situation was met. The proposed model was effective, manage the effects of multipath propagation and reducing complexity by solving malalignment challenges. However, computational complexity occurred when the application required numerous signals.

Cui et al. [11] described an NLOS identification method based on Morlet wave transform and convolutional neural networks (MWT-CNN). They extracted features to transmit time–frequency spectrums from ultra-wideband signals. The online and offline testing processes were divided into two processes. The CNN model was executed to test the extracted features. The study involved extracting features for transmitting time-frequency spectrums from ultra-wideband (UWB) signals. The testing was separated into online and offline processes. The CNN model was utilized to evaluate the extracted features. Both frequency-domain and time-domain UWB signals were analyzed within the proposed model. The results indicated that the performance and accuracy of the model surpassed those achieved by previous methodologies. However, the authors did not consider different scenarios, such as dynamic industrial sites and urban outdoor environments. Zeng et al. [12] proposed a LOS/NLOS identification algorithm based on a convolutional neural network (CNN). The information was processed by the uplink channel for essential processing. Parameters with high precision were identified using the sounding reference signals. The proposed method was identified from pilot symbols by analyzing the features from base station (BS) antennas. The taps were increased, the error rate was reduced, and the performance and complexity were balanced. However, the processing time is high. Hariq et al. [13] demonstrated an NLOS-ultraviolet communication system for spatial diversity techniques. Multiple-input single-output, single-input multiple-output, and MIMO configurations were obtained from the receive and transmit diversity. The different configurations were derived from outage probabilities. The atmospheric turbulence

was increased by executing the link and strength distance performance. However, communication over long distances has to be improved.

To execute green cell-free massive MIMO networks, Femenias et al. [14] described the AP switch ON/OFF algorithm as statically turning the network ON/OFF from the mobile station. The data transmission of downlink and uplink by the spectral and energy efficiency was acquired from mobile stations and access points. Spatial correlation matrices were specified for different antenna arrays to observe the channel model. The different numbers of access points and mobile stations contained varying antenna configurations. The energy efficiency was improved, the access point was reduced, and the transmission antennas were increased. However, the energy efficiency was relatively low and should be improved. To track joint radar communications, Basit et al. [15] used frequency-diverse array MIMO. The radar and communication receiver were tracked to detect the closed-loop design. The beam patterns were range and angle, which contributed only to the angle beam patterns. The security, performance, and bit error rate were improved. The performance in identifying estimation parameters and in tracking was enhanced for radar applications. However, the performance analysis based on different scenarios was not mentioned. García-Morales et al. [16] demonstrated an energy-efficient access point switching to consider nonuniform spatial traffic densities. The spatial traffic heterogeneity was detained in a nonuniform distribution in an analysis of mobile stations. The spatial distribution introduced goodness-of-fit techniques to activate the access points from the network. Large-scale information depended on the spatial location and distribution of access points and mobile stations. The energy efficiency was increased, the approach was robust, and its complexity was reduced. However, an analytical framework that responds to time-varying conditions for the rectification of implementation issues was needed.

Sheikh et al. [17] concentrate on the most productive use of MIMO servo systems. They assume perfect channel state information (CSI) and apply linear precoding algorithms to the small-scale fading (SSF) and large-scale fading (LSF) scenarios. Their results indicate that using the right algorithm to the right channel condition can and does substantially improve system performance. Their findings on user selection in such challenging conditions are particularly relevant to NLOS identification, where the choice of users and the nature of the scattering environment can significantly impact localization accuracy. However, there is no mention of LOS components or non-stationary scattering characteristics. Bakulin et al. [18] propose a method that combines precoding and antenna selection specifically designed for massive multi-user MIMO (MU-MIMO) systems. The proposed method significantly improves signal processing accuracy and system efficiency, making it highly applicable to the domains of localization and channel identification. Through the optimization of antenna selection and precoding techniques, this strategy enhances the system's capability to properly determine channel parameters and improve spatial resolution. These improvements are crucial for achieving precise user localization. This research makes a valuable contribution to enhancing the performance of communication systems and expanding methodologies in localizing and estimating channels in massive MIMO systems. However, varying channel conditions are not explored.

To reduce the effect of NLOS by detecting and identifying whether a corresponding signal is NLOS or LOS in the propagation path, and to accurately position antennas, we propose a novel approach. This solution integrates a CNN-based hybrid Archimedes-based salp swarm algorithm (HASSA, CNN-HASSA) for LOS/NLOS detection with an Ensemble Deep Deterministic Policy Gradient-Based Approach (EDDPG)-based Honey Badger algorithm (HBA) for NLOS mitigation to solve the aforementioned difficulties and improve localization accuracy. The contributions of this work are listed below:

- Different characteristics of channel features are investigated in dynamic environments to develop an efficient LOS identification method, aimed at improving identification accuracy.
- A novel CNN-HASSA method is proposed to enhance localization accuracy in 5G massive MIMO networks by improving the accuracy of LOS identification. The HASSA technique is adopted to address overfitting issues in CNN-based classification.
- The performance of the proposed CNN-HASSA method for LOS/NLOS identification is evaluated and compared with that of MWT-CNN, EFIM, and CNN techniques. These techniques show varying performance when given diverse training elements. The results indicate that the proposed method outperformed other approaches in LOS/NLOS identification.
- The EDDPG-based HBA technique was proposed to mitigate the classified NLOS path. This method provides a new idea for NLOS error mitigation and effectively mitigates the impact of NLOS.

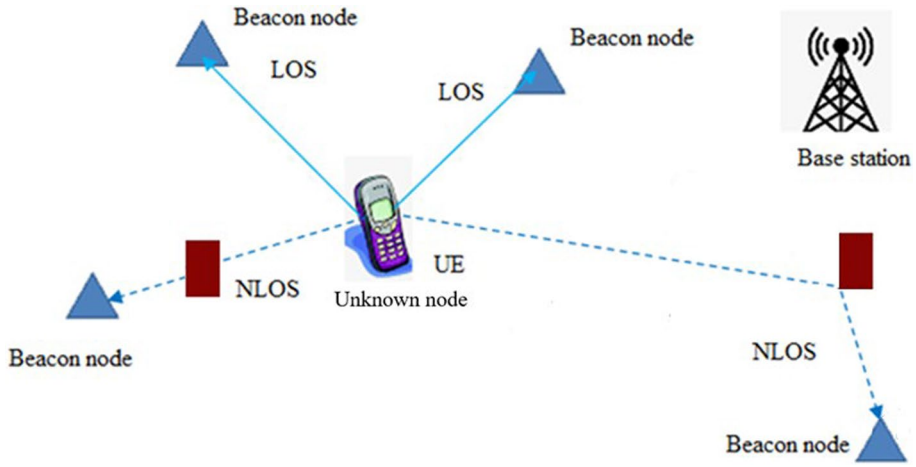

Fig. 1 General system model

The rest of this article is organized as follows: In Sect. 2, the system model of the proposed method is introduced. The identification method for NLOS and LOS is elucidated in Sect. 3. The NLOS mitigation method is described in Sect. 4. The simulation and results are explained in Sect. 5. Section 6 summarizes the paper.

2 System model and problem formulation

Our main objective is to define the presence of LOS/NLOS in the estimated channel features [19]. After the signal propagation environment is determined, various positioning algorithms can be used for localization on the basis of different environments. The LOS/NLOS relies on the location of the transmitter (Tx) and receiver (Rx) and significantly changes its value when Tx and Rx change. The NLOS and LOS propagation for localization is delineated in Fig. 1. We consider a base station in a massive MIMO system equipped with a multitude of antennas to serve a number of users with multiple antennas. We assume the channel is highly scattering and consider it as a Rayleigh fading channel. MIMO systems in Rayleigh fading channels handle fluctuating signal strength due to multipath propagation, enhancing communication reliability and capacity through spatial diversity and multiplexing.

The user transmits pilot symbols to BS for channel estimation. Subsequently, the channel is determined with the matrix transfer function X(f), which is correlated with the parameters of MPCs and can be expressed as

$$X(f) = \sum_{m=1}^{M} \beta_m \cdot \Omega_{Rx}\left(\theta_{Rx,m}\right) \cdot \Omega_{Tx}(\theta_{Tx,m})^T e^{-j2\pi f \varsigma_m} \tag{1}$$

where M refers to MPCs. The Dirac delta function is indicated by $\Omega(\cdot)$. The steering vectors at the transmitter Tx and receiver Rx are indicated by $b_{Tx}\left(\Omega_{Tx,m}\right)$ *and* $b_{Rx}\left(\Omega_{Rx,m}\right)$, respectively. The complex path gain and the delay vector of different paths (TOA) are represented as ρ_m, and ςm, respectively. The transpose operation is denoted as $(\cdot)^T$, and

$$\Omega_{i,m} = \left[cos(\theta_{i,m})sin(\phi_{i,m}), sin(\theta_{i,m})sin(\phi_{i,m}), cos(\phi_{i,m})\right]$$

where $i = 1,2$ denotes the spherical coordinate system's directions/angles; i.e. indicating Tx and Rx, respectively. The azimuth of arrival, elevation of arrival, azimuth of departure, and elevation of departure of the m^{th} path are denoted as $\left(\theta_{i,m}, \phi_{i,m}\right) \in (-\pi, \pi) \times (0, \pi).\theta_{2,m}, \phi_{2,m}, \theta_{1,m}, \phi_{1,m}$. The channel parameters such as delay, power, and the angle of MPCs can be extracted from Eq. (1).

The data are collected by setting the MIMO system, and the features are extracted from the channel between the transmitter and receiver. The extracted features are fed into the CNN for the precise identification of LOS and NLOS. Here, we consider that localization accuracy is the issue. The overfitting issues in the CNN are addressed through the adoption of HASSA. To analyze the localization accuracy, we consider certain parameters such as the AOA of signals, threshold-based TOA, and time difference of arrival, along with the conventional parameters. The mitigation is performed using the reinforcement learning approach.

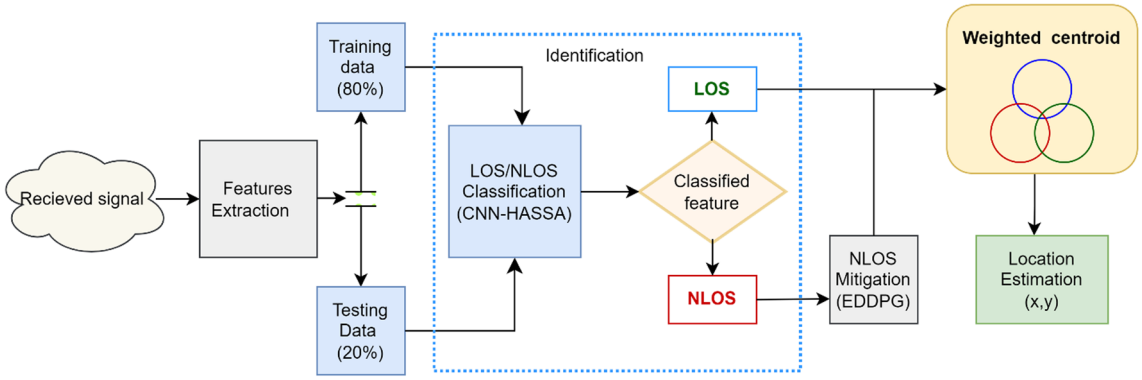

Fig. 2 Overlay of the proposed model

3 Proposed NLOS identification based localization method

This section introduces the proposed method designed to detect LOS and NLOS conditions that occur when a signal is transmitted from one MIMO system to another, such as in V2V communications, where both vehicles (or devices) can act as transmitters and receivers, simultaneously transmitting and receiving signals from each other. Given that a MIMO system is composed of multiple antennas for transmitting and receiving data and in consideration of its dynamic nature, the signal may encounter disruptions, either due to obstacles or natural interference, leading to signal loss. Before mitigation techniques are implemented, distinguishing between NLOS and LOS scenarios is imperative. Accordingly, pertinent features are carefully selected from the channel. The identification of LOS/NLOS conditions is carried out through the utilization of the CNN-HASSA technique. Subsequently, mitigation strategies are applied on the basis of EDDPG-based HBA. To provide a visual representation of the proposed approach, Fig. 2 illustrates a schematic overlay, elucidating the key components and their interactions in a lucid manner.

3.1 Data collection

The presence of LOS/NLOS can be identified by the difference in power delay profiles. When Tx and Rx are in a moving state, the temporal snapshot sequence of $T(T \geq 1)$ is given as $\left[x^{(1)}, x^{(2)}, \ldots, x^{(T)}\right]$. These values ensure significant details about the LOS/NLOS and are used for the identification of them [8].

3.2 Feature extraction

The features from the propagated channels are estimated to analyse the difference between the NLOS and LOS from each snapshot [8]. The selection of channel features for identifying LOS/NLOS status is a tedious task. A framework is developed to avoid manual selection of specific features, allowing the model to learn and extract useful features from input data without the need to manually select specific channels. Our framework utilizes eight channel features to identify LOS/NLOS conditions, capturing various variations in channel conditions and improving the performance in various scenarios. The LOS path is then determined by choosing the features listed below:

- *Highest received power among the delay samples* ($Max(|x^{(t)}|^2)$): The power of NLOS MPC is lesser than that of LOS MPC, and this condition can be utilized for the identification of LOS.
- *Kurtosis of the received power* ($Max(K^{(t)})$): It is used to determine the proportion of fourth- and second-order moments of the amplitude of the received signals and thus estimate the peaks of the amplitude probability distribution function (PDF). It can be formulated as

$$K^{(t)} = \frac{\mathrm{E}\left[\left(|x^{(t)}| - \lambda|x^{(t)}|\right)^4\right]}{\mathrm{E}\left[\left(|x^{(t)}| - \lambda|x^{(t)}|\right)^2\right]^2} = \frac{\mathrm{E}\left[\left(|x^{(t)}| - \lambda|x^{(t)}|\right)^4\right]}{\beta^4_{|x^{(t)}|}} \tag{2}$$

The mean and standard deviation of $|x^{(t)}|$ are given as $\lambda_{|x^{(t)}|}$ and $\beta_{|x^{(t)}|}$ respectively. $\widetilde{x}(t)$ is the average channel response. They can be formulated as

$$\lambda_{|x^{(t)}|} = \frac{\sum_{m=1}^{M} \left||x(t_m)| - |\widetilde{x}(t)|\right|}{M} \tag{3}$$

$$\beta_{|x^{(t)}|} = \sqrt{\frac{\sum_{m=1}^{M} \left(\left||x(t_m)| - |\widetilde{x}(t)|\right|\right)^2}{M}} \tag{4}$$

The amplitude of LOS is higher than that of NLOS. If a larger kurtosis exists, it refers to LOS; if not, it refers to NLOS.

- Received power skewness $\left(\delta^{(t)}\right)$: The symmetric value of the probability distribution can be evaluated by this parameter. The skewness can be expressed as

$$\delta^{(t)} = \frac{\mathrm{E}\left(|x^{(t)}| - \lambda|x^{(t)}|\right)^3}{\beta^3_{|x(t)|}} \tag{5}$$

The skewness of NLOS is higher than that of LOS. That is, the skewness of the Rayleigh distribution is greater than that the Rician distribution.

- Rising time $\left(\Delta\imath^{(t)}\right)$: It is the estimation of the time period between the first MPC and the strongest MPC. It can be formulated as

$$\Delta\imath^{(t)} = \underset{\imath}{argmax}\left|x^{(t)}\right| - min\left(\imath_m\right) \tag{6}$$

The rising time of NLOS components is greater owing to the fact that the first component in NLOS has been attenuated with the strongest diffractions. Moreover. The index of the MPCs is given as m, and the time delay is denoted as ı.

- Root mean square (RMS) delay spread $\imath^{(t)}_{rms}$: It can be used to estimate the overall RMS delay spread for all the components in MPCs in the current snapshots. It can be measured using the following equations:

$$\imath^{(t)}_{rms} = \sqrt{\frac{\sum_{m=1}^{M}\left(\imath^t_m - \imath^{(t)}_l\right)^2\left|x^{(t)}_m\right|^2}{\sum_{m=1}^{M}\left|x^{(t)}_m\right|^2}} \tag{7}$$

The excess mean delay is indicated as $\imath^{(t)}_l$ and can be formulated as

$$\imath^{(t)}_l = \frac{\sum_{m=1}^{M}\imath_m\left|x^{(t)}_m\right|^2}{\sum_{m=1}^{M}\left|x^{(t)}_m\right|^2} \tag{8}$$

The NLOS channel does not carry LOS, and it exhibits greater RMS delay spread than the LOS channel.

- Rician K-factor $R^{(t)}_s$: It can be defined as the proportion of dominant power MPCs and residual power MPCs. If the situation is NLOS, $R^{(t)}_s$ will become zero; a positive value indicates the LOS situation. It can be expressed as

$$R^{(t)}_s = \frac{\left(|x^{(t)}|_{max}\right)^2}{2\beta^2_{|x^{(t)}|}} \tag{9}$$

The amplitude of the maximized peak snapshot is indicated as $\left|x^{(t)}\right|_{max}$ and the variance of the amplitude is denoted as $\beta_{|x^{(t)}|}$.

These features are utilized by many researchers to identify LOS and NLOS effectively. However, the identification of LOS and NLOS still requires some improvement. Hence, we consider temporal and static angular features along with those features. These added features are explained below.

- Angular spread of departure/arrival $\left(\eta_{ASD}^{(t)}/\eta_{ASA}^{(t)}\right)$: The spread of AOA and AOD is estimated for all MPCs with each snapshot. This feature can be formulated as

$$\eta_{ASD}^{(t)}/\eta_{ASA}^{(t)} = \sqrt{\frac{\sum_{m=1}^{M}\left|exp\left(i\theta_{1/2,m}^{(t)}\right) - \lambda_{\theta 1/2}^{(t)}\right|^2\left|x_m^{(t)}\right|^2}{\sum_{m=1}^{M}\left|x_m^{(t)}\right|^2}} \tag{10}$$

The mean direction of the Power angular spectrum is indicated as $\lambda_{\theta 1/2}^{(t)}$ and evaluated as

$$\lambda_{\theta 1/2}^{(t)} = \frac{\sum_{m=1}^{M} exp\left(i\theta_{1/2,m}^{(t)}\right)\left|x_m^{(t)}\right|^2}{\sum_{m=1}^{M}\left|x_m^{(t)}\right|^2} \tag{11}$$

The angle spread of the NLOS condition is higher than that of the LOS condition.

- Angular Difference $\left(\Delta\eta_m^{(t)}\right)$: The variations in AOA $\left(\theta_2\right)$ and AOD $\left(\theta_1\right)$ are estimated from the strongest MPC. For the LOS condition, the strongest MPC must be LOS MPC. Eventually, the signal must be directly propagated from Tx to Rx in LOS MPC and thus remains constant. The angular difference in NLOS MPC is dynamic and changes with movement. The angular difference can be evaluated as

$$\Delta\eta_m^{(t)} = \left|e^{(i\theta_{1,m,\max}^{(t)})} - e^{(i\theta_{2,m,\max}^{(t)})}\right| \tag{12}$$

- Angular Variant of departure/arrival $\left(\Delta\chi^{\theta_{1,(t)}}\right), \left(\Delta\chi^{\theta_{2,(t)}}\right)$: This quantifies the variation of the AOD and AOA of the strongest path within a specified time interval. The AOD/AOA of the strongest path of a snapshot is denoted as $\theta_{1/2}$, and its variant at time interval Δt can be formulated as

$$\Gamma_{\theta_{1/2}}^{(t)} = \left[\theta_{1/2}^{(t-\Delta t)}, \theta_{1/2}^{(t-\Delta t-1)}, ..., \theta_{1/2}^{(t)}\right]^T \tag{13}$$

Equation (13) can be modified to a matrix to provide a systematic way of extracting specific elements and can be rewritten as

$$\Gamma_{\theta 1/2}^{(t)} = \begin{bmatrix} rsin\theta_{1/2}^{(t-\Delta t)} & rcos\theta_{1/2}^{(t-\Delta t)} \\ . & . \\ . & . \\ . & . \\ rsin\theta_{1/2}^{(t)} & rcos\theta_{1/2}^{(t)} \end{bmatrix} = [\partial 1, \partial 2] \tag{14}$$

Equation (14) implies that the variant of AOD/AOA can be understood as a combination of two vectors, ∂1 and ∂2. To infer the dispersion of AOA and AOD in the strongest path we consider the eigenvalue of the covariance matrix of $\Gamma_{\theta 1/2}^{(t)}$ in this condition which can be expressed as

$$\chi^{\theta_{1,/2(t)}} = \sum eigen\left(\begin{bmatrix} cov(\partial 1, \partial 1) & cov(\partial 1, \partial 2) \\ cov(\partial 2, \partial 1) & cov(\partial 2, \partial 2) \end{bmatrix}\right) \tag{15}$$

The total features from the channel are given as

$$\wp^{x(t)} = \left\{ max\left(\left| x^{(t)} \right|^2 \right), K^{(t)}, \delta^{(t)}, \Delta\iota^{(t)}, \iota_{rms}^{(t)}, R_s^{(t)}, \Delta\eta_m^{(t)}, \eta_{ASD}^{(t)}, \eta_{ASA}^{(t)}, \Delta\chi^{\theta_{1(t)}}, \Delta\chi^{\theta_{2(t)}} \right\} \tag{16}$$

3.3 Proposed CNN based approach for the localization

CNNs are frequently employed in computer vision applications like segmentation, object detection, and image categorization. They can be trained to analyze input data, which could be images or signals. CNNs are utilized for the effective classification of features. Here, we adopt a CNN to detect LOS and NLOS conditions with inclusion localization as the detection problem. The main aim of our proposed method is explained in two stages: (i) training and (ii) localization stages. During the former stage, the features gathered from the previous stages are trained. In the latter stage, the features from the MIMO system are forwarded to the trained neural network, and the location is evaluated with the weighted output value from the output layer. This article presents the CNN framework, along with the loss function and training approach.

3.3.1 CNN framework

The proposed framework is inspired by LeNet and AlexNet, which can be exploited to detect considerable features. From Fig. 3, the proposed CNN contains five layers, including two fully connected layers and three convolutional layers. The proposed CNN is different from the traditional one in the usage of channel impulse response features. The features are padded before feeding into the convolutional layer to avoid size reduction [20]. The channel impulse response features are small in size and must be sustained throughout the process. Pooling layers are not included in this process in consideration of their intricate behavior. The extracted features can be used to provide enhanced location features; hence, pooling layers are not needed. Here, we set 10 convolutional kernels and select a 5×5 filter size. The padding of input features is performed, and the stride of the filter is set to 1 to derive the exact time–frequency information.

Predominantly, we adopt an activation function, rectified linear unit (ReLU), that can be used for the nonlinearity function in CNN. It increases the computational speed while conducting the detection process. ReLU can be given as

$$h(y) = max(0, y) \tag{17}$$

The number of reference points affects the neurons in the output layer. If the targeted device appears in the reference points, then softmax will act as the activation function. The softmax function can be expressed as

$$z^{(j)} = \frac{exp(w_j^T y^{(i)})}{\sum_{j=1}^{V} exp(w_j^T y^{(i)})} \tag{18}$$

V is used to denote the output neurons and is equal to the number of reference points. The j^{th} neuron from the output layer is indicated as $z^{(j)}$ here the output neurons index is j. $y^{(i)}$ is the second last layer in the output layer and the weight

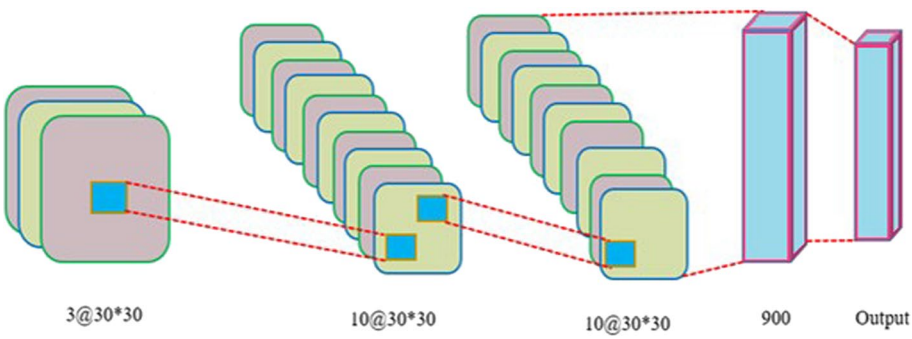

Fig. 3 Framework of proposed CNN for localization

vector used to connect the second last and output layers is indicated as w_j. The transformation is indicated as T, and the softmax function maps in the range of [0, 1].

The loss function is used to train CNN. We utilize the cross-entropy incorporated with the regularization function, which can be expressed as

$$L(w) = -\frac{1}{U}\left[\sum_{i=1}^{U}\sum_{j=1}^{V} I\left\{s^{(i)} = j\right\} log \frac{exp\left(w_j^T y^{(i)}\right)}{\sum_{i=1}^{V} exp\left(w_m^T y^{(i)}\right)}\right] + \frac{\eta}{2}\sum_{i=1}^{D}\sum_{j=1}^{V} w_{ij}^2 \tag{19}$$

The weight of the regularizer is indicated as η, and it must be greater than zero. The dimensionality of w_j is denoted as D, which respects the number of neurons in the second last layer. The indicator function is represented as $I\{\}$. The training dataset size is indicated as U, and the index of the reference points is $s^{(i)}$. To overcome the overfitting issues in CNN, we utilize HASSA, which will be explained in the next section.

3.3.2 SSA

The collective behavior of salps while foraging and navigating in oceans inspires a new swarm algorithm called SSA. During foraging, salps arrange in chains to attain excellent locomotion [21]. Random positions with multiple salp sets are initialized on the basis of other swarm algorithms. SSA is divided into a leader's and followers' classes. The leader is represented as the first salp that is present in the salp chain, and the remaining are described as followers. The position of salps in the m-dimensional search space is determined. The swarm targets are indicated by these salp searches for food source. The equation expresses the salp leader's action and frequently updates the position.

$$Y_i^l = \begin{cases} FS_i + D_1\left(\left(U_i - L_i\right) \times D_2 + L_i\right), D_3 \le 0 \\ FS_i - D_1\left(\left(U_i - L_i\right) \times D_2 + L_i\right), D_3 > 0 \end{cases} \tag{20}$$

Within the i^{th} dimension, the leader position is Y_i^l and FS_i is the food source. The upper and lower bounds in the *ith* dimension are U_i and L_i, respectively. The random numbers are D_2 and D_3 that tend to the interval as [0, 1]. In this SSA, the significant coefficient parameter is D_1. The following equation calculates the coefficient parameter D_1 that makes a balancing in the exploration and exploitation stages.

$$D_1 = 2e^{-\left(4T/T_{max}\right)} \tag{21}$$

The current and maximum number of iterations are T and T_{max}, respectively. SSA updates the position of followers after updating the position of the leader, as shown below:

$$Y_i^j = \frac{1}{2}\left(Y_i^j + Y_i^{j-1}\right) \tag{22}$$

Within the i^{th} dimension, the j^{th} follower's position is Y_i^j, which is greater than 1. The algorithm is expressed via a pseudocode.

3.3.3 Archimedes optimization (AO) algorithm

A partially or fully immersed object in a fluid inspires Archimedes' principle or the AO algorithm [22]. The mathematical model of the AO method is explained below.

- Initialization:

Equation (23) initialize all objects' positions. M_2 objects population in the i^{th} position is O_i. In the search space, the upper and lower bounds are U_i and L_i, respectively.

$$O_i = L_i + random \times \left(U_i - L_i\right); i = 1,2, \ldots, M_2 \tag{23}$$

For every i^{th} object, the initial density and volume are D_i and V_i, respectively.

$$D_i = random \tag{24}$$

$$V_i = random \tag{25}$$

where random is a d-dimensional vector that is randomly generated within the interval [0, 1]. Equation (26) initializes the *ith* object acceleration *A*.

$$A_i = L_i + random \times \left(U_i - L_i\right) \tag{26}$$

The best fitness values with the objects are selected, and the initial population is evaluated. A_{best}, V_{best}, D_{best} and y_{best} are allocated.

- Volume and density updating:

On the basis of the i^{th} object, the volume and density for the iteration $T+1$ are updated and expressed as follows:

$$V_i^{T+1} = V_i^T + random \times \left(V_{best} - V_i^T\right) \tag{27}$$

$$D_i^{T+1} = D_i^T + random \times \left(D_{best} - D_i^T\right) \tag{28}$$

The volume and density associated with the best object are V_{best} and D_{best}, respectively. A uniformly distributed random number is denoted as *random*.

- Density factor and Transfer operator:

After a time period, collision occurs among the objects. C^T is the density decreasing factor. It is aids AO in transitioning from global to local search, which is diminishes with time as

$$C^T = \exp\left(T - T_{max}/T_{max}\right) - \left(T/T_{max}\right) \tag{29}$$

C^T diminishes over time, facilitating convergence in previously identified favorable areas. The current and maximum numbers of iterations are T and T_{max}, respectively. From the exploration to exploitation, the transfer operator (*TRO*) implements the AO algorithm and transforms the search.

$$TRO = \exp\left(T - T_{max}/T_{max}\right) \tag{30}$$

TRO is gradually increased to reach the maximum time 1.

- Exploration and exploitation stage:

Collision among objects occurs if $TR0 \leq 0.5$. For $T+1$ iteration, Eq. (31) updates the acceleration that selecting random materials (*RM*).

$$A_i^{T+1} = \frac{D_{RM}^{(i)} + V_{RM}^{(i)} \times A_{RM}^{(i)}}{D_i^{T+1} \times V_i^{T+1}} \tag{31}$$

The random materials with respect to acceleration, density, and volume are A_{RM}, D_{RM} and V_{RM}, respectively.
No other collision exists among the objects if $TR0 > 0.5$. For $T+1$ iteration, Eq. (32) updates the object's acceleration.

$$A_i^{T+1} = \frac{D_{best}^{(i)} + V_{best}^{(i)} \times A_{best}^{(i)}}{D_i^{T+1} \times V_i^{T+1}} \tag{32}$$

The best object acceleration is A_i^{T+1}.

- Acceleration normalization and position updating:

Equation (33) calculates the percentage of acceleration normalization. It determines the percentage of adjustment for every agent.

$$A_{i-NR}^{T+1} = \alpha \times \frac{A_i^{T+1} - min(A)}{max(A) - min(A)} + J \tag{33}$$

The normalization range are J and α, which are set to 0.1 and 0.9, respectively. For the next iteration $T+1$, the i^{th} object position if $TRO \leq 0.5$, and the following equation updates the object position.

$$y_i^{T+1} = y_i^T + E_1 \times random \times A_{i-NR}^{T+1} \times C^T \times \left(y_{random} - y_i^T\right) \tag{34}$$

A value of 2 is set for constant E_1. Equation (35) updates the object position if $TRO > 0.5$.

$$y_i^{T+1} = y_{best}^T + FL \times E_2 \times random \times A_{i-NR}^{T+1} \times C^T \times \left(f \times y_{best} - y_i^T\right) \tag{35}$$

where $f = E_3 \times TRO$. f increases with time, and constant E_2 is set to 6. The motion direction change via a flag is given as follows:

$$FL = \begin{cases} 1, if R \leq 0.5 \\ 0, if R > 0.5 \end{cases} \tag{36}$$

From the above equation, $R = 2 \times random - E_4$. E_4 is a constant value, typically recommended to be set at 0.5. The best solution with the objective function of every object is evaluated.

3.3.4 HASSA

SSA encounters several challenges in determining the best solution because of its complexity, slow convergence, slow diversity, premature convergence, and time consumption [23, 27]. Nevertheless, SSA may be able to deal with complex functions when the detection and exploitation costs are considerably high. In this study, the follower position updating stage of SSA is improved by using the transfer operator of the AO algorithm to solve the complicated optimization functions. In the search domain, the optimum solution detection stage is exploited with respect to SSA. The best global performance is achieved, and the local optimum is neglected. The novel algorithm called HASSA shows a better convergence rate in solving optimization problems. HASSA integrates the idea of buoyant force based on Archimedes' principle to improve the swarm's ability to search. The model is explained as follows:

- *Encoding the population:* The binary encoding encodes the population of HASSA and represents every vector as a string of 0 and 1. The binary values of 0 represent the unselected appropriate solution and 1 means selecting the suitable solution.
- *Initialization:* The parameters of SSA and AO algorithm are initialized with a maximum number of iterations.
- *Population updating:* The population updating during the exploration and exploitation stage is performed via SSA and AO algorithms. The probability value below indicates the particular algorithm selection.

$$Pro_j = \frac{F_j}{\sum_{k=1}^{m} F_j} \tag{37}$$

The transfer operator is updated during the follower position updating phase of SSA. The optimal best solution is obtained with a high convergence rate. The conditions and random factors introduced in the position update help to guide the search process effectively. Within the i^{th} dimension, the new leader position denotes as

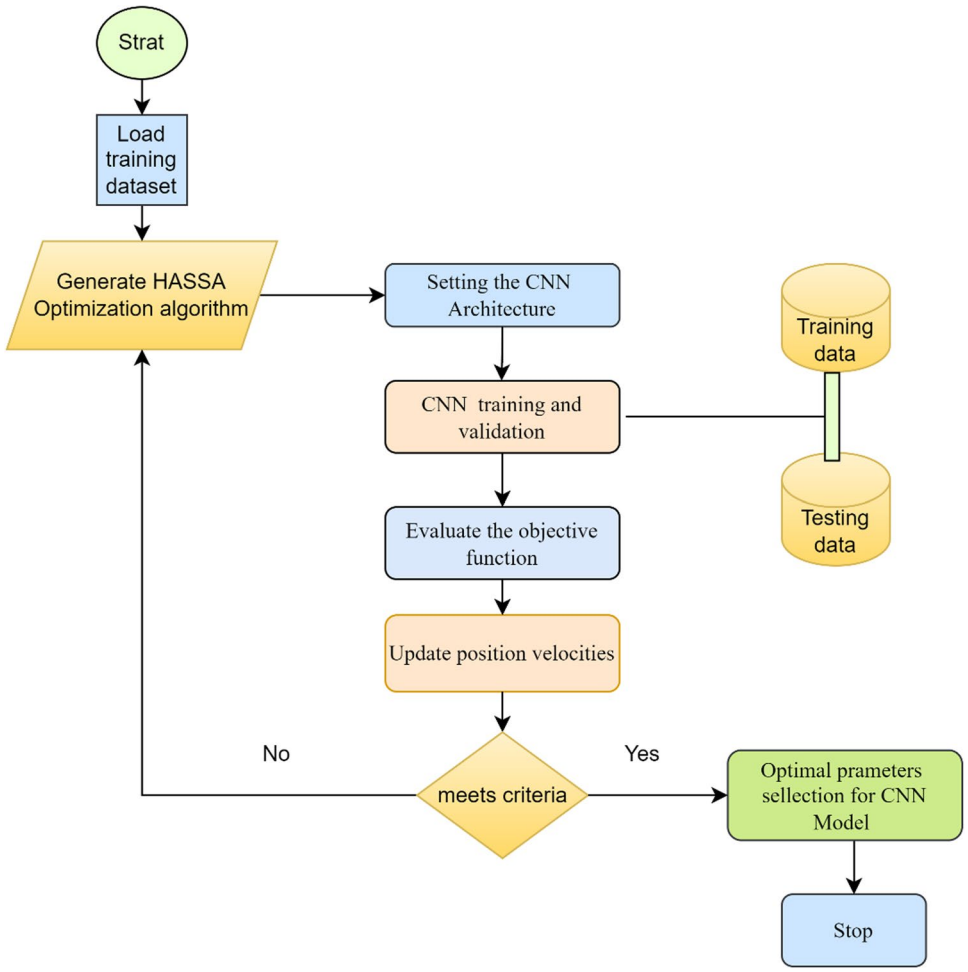

Fig. 4 The proposed CNN-HASSA Identification Method flow chart

$$Y_{new,i}^{l} = \begin{cases} Y_{old,i} + rand_j\left(New_{mean} - TRO * Mean_i\right), D_3 < 0 \\ FS_i + D_1\left(\left(U_i - L_i\right) \times D_2 + L_i\right), D_3 \le 0 \\ FS_i - D_1\left(\left(U_i - L_i\right) \times D_2 + L_i\right), D_3 > 0 \end{cases} \tag{38}$$

3.3.5 CNN-HASSA based localization

In consideration of the benefits of both strategies, CNN and the Archimedes-based SSA are coupled. The CNN can conduct feature extraction and classification, and the swarm algorithm can improve the CNN's performance by optimizing its hyperparameters. The CIR features extracted from the channel are forwarded to the CNN structure in the proposed localization stage [25, 28]. Through a hybrid method, the overarching goal is to increase the reliability and effectiveness of NLOS identification. When the targeted MIMO is any location of the interested area, the position can be estimated with the weighted centroid approach and can be formulated exactly as

$$\widetilde{P} = \frac{\sum_{j\in\Psi} z^{(j)} Q_j}{\sum_{j\in\Psi} z^{(j)}} \tag{39}$$

The coordinate of the j^{th} reference point is denoted as Q_j. The deemed reference points are represented as Ψ. The CNN hypertuning procedure utilizing HASSA is shown in Fig. 4 as a flow chart. After the location-specific NLOS and

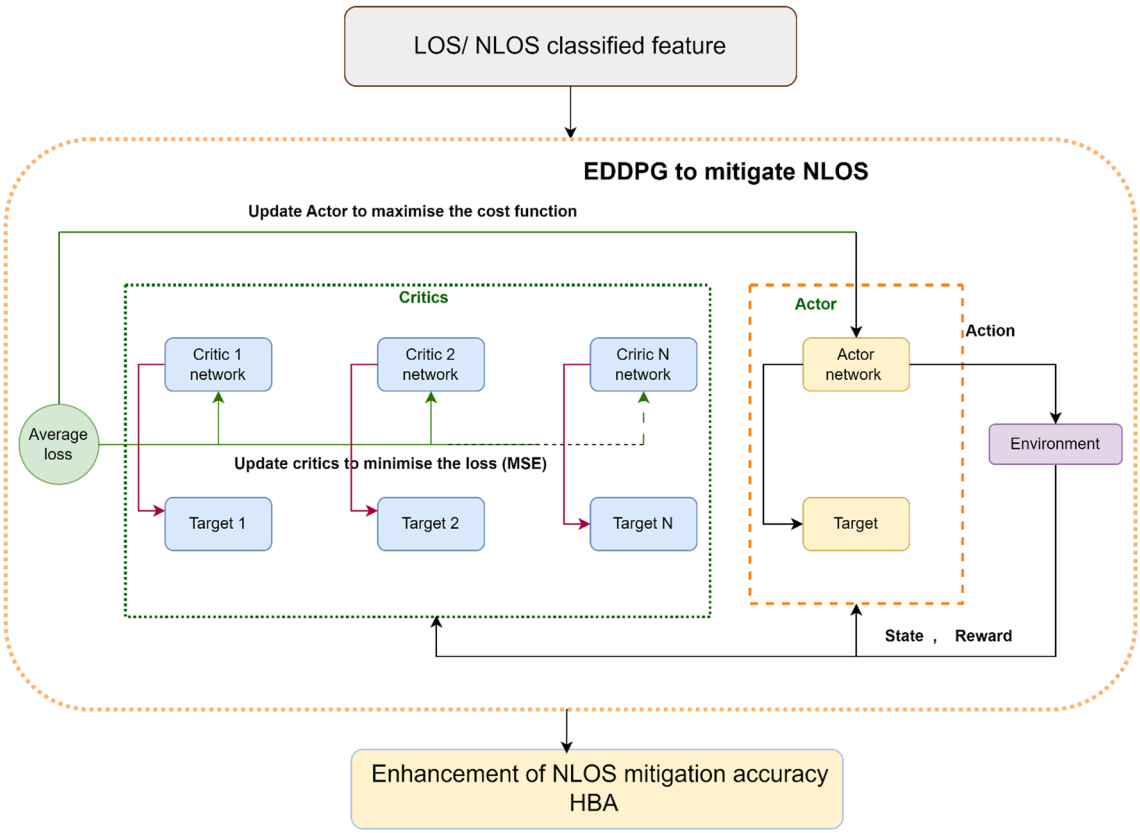

Fig. 5 The flow chart of the proposed mitigation model

LOS conditions of signals are determined, the NLOS must be mitigated to efficiently receive signals from Tx. To this end, we adopt EDDPG-based HBA. The following section elucidates the mitigation process.

4 EDDPG-HBO for the mitigation of NLOS

4.1 Ensemble deep deterministic policy gradient (EDDPG)

The Deep Deterministic Policy Gradient (DDPG) is an amalgamation of Q learning and policy gradient. There are four networks in DDPG: the critic network, actor network, target critic network, and target actor network. The critic network utilizes the loss function to update the Q function, enabling DDPG to effectively handle intricate and continuous actions. In this work, the continuous issues describe the parameters and environment involved in localization and NLOS mitigation, becoming persistent in the context of addressing these challenges. The state space environment involves parameters like distance, angle, and object position, which define the continuous state space. The continuous variables represent object positions such as transmitters, receivers, landmarks, and obstacles, according to the continuous coordinate system. The continuous action space included receiver gain, antenna orientation, and transmit power parameters related to the localization and NLOS mitigation processes. Such actions do not represent discrete decisions; instead, they are modifications on a continuous scale. For this reason, the general reinforcement learning model is not directly applicable to continuous action spaces and discrete states. The Ensemble Deep Deterministic Policy Gradient-Based Approach (EDDPG), an extended version of the DDPG algorithm, improves performance and convergence to address the challenges of continuous action spaces. It's a modified version of DDPG. Agents in continuous action spaces train using the EDDPG reinforcement learning algorithm. The model-free, off-policy reinforcement learning algorithm EDDPG is similar to DDPG in that it learns a deterministic policy function to map state-action pairs to Q-values and updates the policy function utilising the policy gradient approach. In a continuous and complex environment, EDDPG enhances localization accuracy and adjusts for NLOS effect mitigation. Figure 5

illustrates the mitigation process of NLOS. The proposed approach is based on a single-actor multi-critic structure [24, 27]. The figure illustrates the application of EDDPG to enhance the precision of NLOS mitigation, with N representing the number of critics.

Although EDDPG was not explicitly developed for NLOS mitigation, it can be successfully modified for this objective. The crucial aspect lies in precisely identifying the problem and customizing the strategy to suit your specific application. When dealing with NLOS situations, EDDPG takes into account several aspects, such as signal strength, multipath attenuation, diffraction, reflections, obstacle roughness, and distance. In order to obtain the best possible performance, EDDPG functions inside a state space that encompasses both channel quality and the Received Signal Strength (RSS) associated with NLOS features. In NLOS scenarios, the reward function encourages activities that enhance communication performance by improving the data transfer rate, limiting the number of lost packets, and maximizing the intensity of the signal. EDDPG utilizes the action space to make decisions regarding adjustments to transmission parameters, such as modulation schemes, frequency allocation, antenna orientation, and transmit power.

In LOS conditions, the received signal strength is typically stronger because there is a direct path between the transmitter and receiver, whereas in NLOS conditions, obstacles or reflections weaken the received signal strength. The step of loss estimation involves estimating the strength of the signal received by the agent. This is important because the strength of the signal will affect the agent's ability to take actions and achieve its goals. RSS can be continuously monitored, allowing the EDDPG to adapt its mitigation strategy based on changes in the environment. Fluctuations in RSS might indicate moving obstacles or varying channel conditions, prompting the EDDPG to adjust its chosen action accordingly. While in the cost function step involves calculating the cost of taking a particular action. The cost function is typically based on the difference between the desired outcome and the actual outcome. In this case, the mean squared error (MSE) is used to measure the difference between the estimated and actual receiver signal strength. EDDPG can evaluate the typical amount of signal loss that occurs in NLOS conditions (average NLOS loss) and use this information to mitigate the impact on received signal strength by analyzing the actual received signal strength. By using the average NLOS loss as a reference, EDDPG can analyze the current RSS to make informed decisions about mitigating the negative effects of NLOS propagation. Enhancement of mitigation accuracy achieves using Honey Badger algorithm, this step involves using the Honey Badger algorithm to improve the accuracy of the NLOS mitigation process. The Honey Badger algorithm is a swarm intelligence algorithm that can be used to optimize complex systems [26, 28]. In this case, it is used to optimize the parameters of the EDDPG algorithm to improve its performance. The stableness of the algorithm is enhanced by the estimation of gradient evaluation after the completion of the policy integration network. Let us assume that the quantity of evaluation networks utilized is N.

The average value of the NLOS propagation loss related MIMO system can be calculated as

$$B_{mean}(s,a|\varphi) = \frac{1}{N}\sum_{i=1}^{N} B_i(s,a|\varphi) \tag{40}$$

$$B_{mean}^{Tar}(s,a|\varphi^{-}) = \frac{1}{N}\sum_{i=1}^{N} B_i^{Tar}(s,a|\varphi_i^{-}) \tag{41}$$

The critical NLOS loss and targeted NLOS loss in the output are indicated as $B_i(s,a|\varphi)$ and $B_i^{Tar}(s,a|\varphi_i^{-})$, respectively. The parameters for the representation of critical and targeted NLOS losses are given as φ, and φ_i^{-}. The state, action, and discount factor indicated as s, a, and ε, respectively. Moreover, the average loss and cost function are evaluated as

$$\omega = m(s,a) + \varepsilon B_{mean}^{Tar}(s,a|\varphi^{-}) - B_{mean}(s,a|\varphi) \tag{42}$$

$$H_{mean}(\varphi) = \left(m(s,a) + \varepsilon B_{mean}^{Tar}(s',a'|\varphi^{-}) - B_{mean}(s,a|\varphi)\right)^2 \tag{43}$$

The average NLOS loss is evaluated and can be mitigated by deeming the received signal strength. The cost function of the NLOS loss can be evaluated with the additional term known as the mean square error value. This can be used to reduce the loss function in the i^{th} evaluation as

$$H(\varphi_i) = \gamma H_{mean}(\varphi) + \kappa H_{td_i}(\varphi_i) + \epsilon\left(B_i\left(s,a|\varphi_i\right) - B_{mean}(s,a|\varphi)\right)^2 \tag{44}$$

The weight coefficients are indicated as γ and κ. The policy and penalty factor are indicated as μ and ϵ. H_{td_i} the cost function out of loss. Then the gradient evaluation can be defined as

$$\nabla_{\varphi_\Pi} L(\varphi) = E_{n_t \in \sigma^\kappa}\left[\nabla_\gamma B_{mean}\left(s, a\middle|\varphi^B\right)|_{s=s_t\ ,\ \ a=\mu\left(s_t|\varphi^\mu\right)}, \nabla_{\varphi_\mu}(s\middle|\varphi^\mu)|_{s=s_t}\right] \tag{45}$$

The mitigation of NLOS can be achieved by the reduction of cost function and loss function and further the mitigation accuracy can be increased with the utilization of the HBO algorithm. This is explained in the next section.

4.2 Honey badger algorithm (HBA)

The white and black fluffy fur of mammals often determined in the rainforests of Africa and semi-deserts are called Honey badger. Both exploitation and exploration equip the HBA thereby referring to the global optimization model. The mathematical modelling of HBA [26] is delineated as in the following.

$$CSP = \begin{bmatrix} Y_{11} & Y_{12} & Y_{13} & \cdots & Y_{1d} \\ Y_{21} & Y_{22} & Y_{23} & \cdots & Y_{2d} \\ \vdots & \vdots & \vdots & \vdots & \vdots \\ Y_{m1} & Y_{m2} & Y_{m3} & \cdots & Y_{md} \end{bmatrix} \tag{46}$$

$$Y_j = \left[Y_j^1, Y_j^2, ..., Y_j^d\right] \tag{47}$$

The candidate solution population is CSP and Y_j is the j^{th} honey badger position.

- Population initialization:

The seven variables, r_1 to r_7, which are identically independent uniformly distributed in the interval [0, 1]. Based on the position, the number of population sizes or honey badgers (M) is initialized and explained as follows:

$$Y_j = L_j + r_1 \times \left(U_j - L_j\right) \tag{48}$$

The upper and lower bounds of search space are U_j and L_j. The candidate population size is M and the j^{th} honey badger position is Y_j.

- Intensity definition (ID) and factor updating:

The prey strength concentration correlates to the intensity and the prey smell intensity is ID_j. Depending upon the Inverse Square Law, the motion will be fast if the smell is high.

$$ID_j = r_2 \times \frac{G}{4\pi d_j^2} \tag{49}$$

$$G = \left(Y_j - Y_{j+1}\right)^2 \tag{50}$$

$$d_j = Y_{prey} - Y_j \tag{51}$$

The strength of the source is G and the distance between the j^{th} badger and prey is d_j. The smooth transition from exploration to exploitation is ensured by using a density factor ζ that manages the time-varying randomization.

$$\zeta = n \times exp\left(\frac{-T}{T_{max}}\right) \tag{52}$$

The current and maximum iterations are T and T_{max}. The constant is n.

- Agents' position updating:

Equation (53) expresses the cardioids motion that is performed via honey badger in the digging phase.

$$Y_{new} = Y_{prey} + FL \times \delta \times ID \times Y_{prey} + FL \times r_3 \times \zeta \times d_j \times \left| cos\left(2\pi r_4\right) \times \left[ID - cos\left(2\pi r_5\right)\right]\right| \tag{53}$$

The prey position is Y_{prey} and FL is the flag.

$$FL = \begin{cases} 1\,, if\ r_6 \leq 0.5 \\ -1\,, Otherwise \end{cases} \tag{54}$$

Equation (55) indicates that a honey badger conducts searches in proximity to the prey location Y_{prey} identified thus far, utilizing distance information d_j. Equations (52) and (54) determines the ζ and FL, respectively. At this juncture, the search is affected by time-varying in search behavior ζ. The two random r_6 and r_7 are values within the range of 0 to 1.

$$Y_{new} = Y_{prey} + FL \times r_7 \times \zeta \times d_j \tag{55}$$

After mitigating the NLOS we have evaluated the Cumulative Distribution function (CDF) [27] for the estimation of residual error in the MIMO network.

5 Simulation and results

This section presents the simulation setup and collected dataset and the performance analyses in a detailed manner.

5.1 Simulation setup

To analyse the performance, we have used vehicle-to-vehicle communication. We model an urban environment with an area of 100 m × 300 m. The distance between the base station (BS) and the user (vehicle) varies from 20 to 150 m. This setup is used to evaluate communication performance and localization accuracy across different distances within a realistic urban setting. Here the NLOS arises while the vehicle is moving, buildings, infrastructure, and more. The LOS occurs naturally. However, the main reasons for the formation of NLOS are the same and the channel features are different. Moreover, the inclusion of noises also affects the detection accuracy. The following section will analyze the impact of feature selection from the channel. The parameter settings of the proposed CNN is depicted in Table 1.

5.2 Impact of feature selection

Various positions, along with streets, contribute differently to every channel feature for the identification of LOS and NLOS. From the measurement data, the extraction of the probability distribution function (PDF) of various channel

Table 1 CNN Parameter settings

Type of layer	Size of input	Parameters	Function
Convolutional layer)	30 × 30 × 3 Stride = 1 Pad = 2	Filter kernel = 5 × 5 Features = 10	ReLUs
Convolutional layer	30 × 30 × 10 Stride = 1 Pad = 2	Filter kernel = 5 × 5 Features = 10	ReLUs
Convolutional layer	30 × 30 × 10 Stride = 1 Pad = 2	Filter kernel = 5 × 5 Features = 10	ReLUs
FC layer	9000	Neurons = 900 50% dropout	ReLUs
FC layer	900	Neurons number RP	Softmax

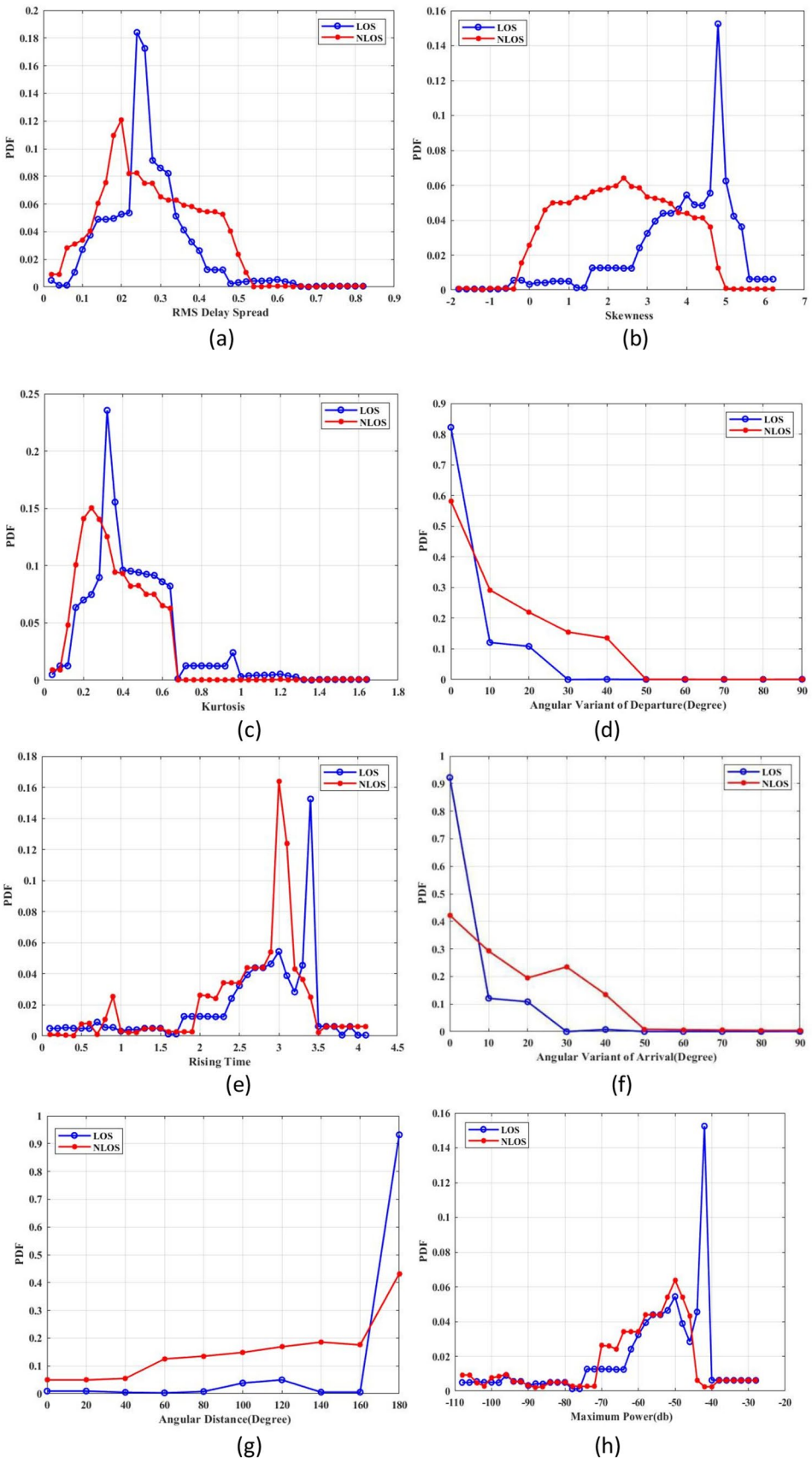

Fig. 6 PDF of various channel features: **a** Skewness, **b** RMS delay spread, **c** Kurtosis, **d** Angular variant of departure, **e** Rising time, **f** Angular variant of arrival, **g** Angular distance and **h** Maximum power

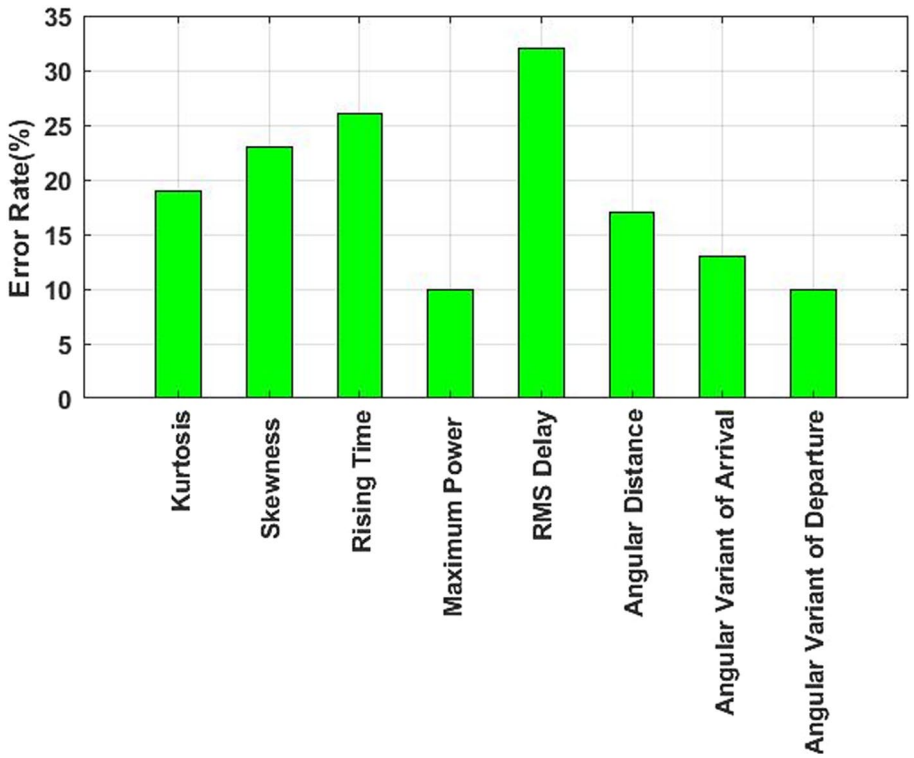

Fig. 7 Different features with their error rate

Table 2 Features types

Type	Features
Conventional	$Max\left(\left\|x^{(t)}\right\|^2\right), K^{(t)}, \delta^{(t)}, \Delta\iota^{(t)}$
Static (Angular)	$\eta_m^{(t)}, \eta_{ASD}^{(t)}, \eta_{ASA}^{(t)}$
Time Varying (Angular)	$\Delta\chi^{\theta_{2,(t)}}\chi^{\theta_{1,(t)}}$

Table 3 Features Settings

Sets	Conventional features	Static (angular)	Time varying angular
Set 1	✓		
Set 2		✓	✓
Set 3	✓		✓
Set 4		✓	
Set 5	✓	✓	✓
Set 6	✓	✓	

features is plotted in Fig. 6. Various PDFs of these features have been shown and the following figures are indeed the NLOS and LOS channels. The K-fold validation is widely used to evaluate the performance of identification more correctly.

The K disjoint sets $Y = \{Y_1 \cup Y_2 \cup .... \cup Y_K\}$ and $Y_j \cap Y_i = \varphi$ divides every dataset into Y^l and Y^g.
The set Y_j is used to evaluate and impose the training depending upon Y/Y_j.
For every $i = 1,\ldots. K$, the results are revalidated. The trade-off between both accuracy and computational complexity is considered.

Each feature deterministic threshold evaluates the performance of identification to be fully contrasted to traditional solutions.

The probability density functions (PDFs) depicting the statistical distributions of the mentioned channel properties are illustrated in Fig. 6. A close examination of the figure reveals a notable disparity in the probability distributions of these features in LOS and NLOS situations. These distinct patterns suggest that the analyzed features, while exhibiting some areas of overlap, encapsulate valuable information for precise differentiation between LOS and NLOS conditions. Let $c \in C = \{0,1\}$, where $c = 0$ and $c = 1$ correspond to the states of NLOS and LOS, respectively. The objective is to accurately ascertain a user's LOS/NLOS state on the basis of the provided channel information. Various identification error rates with different features are depicted in Fig. 7. The error rate for identification is 10% with respect to a maximum variant of departure, and the maximum power is achieved. The figure displays the maximum error rate for the RMS delay scenario and the minimum error rate for the maximum received power scenario. High received power generally indicates a strong signal, which can significantly improve the signal-to-noise ratio (SNR). A high SNR makes the signal distinguishable from noise, leading to accurate identification of the NLOS condition. Consequently, the high signal strength enhances SNR, making NLOS conditions easy to identify and resulting in low error rates. On the contrary, scenarios with a high RMS delay spread maximize the error rate. We can use the RMS delay spread to estimate the overall delay dispersion for all components in the multipath components (MPCs) of the current snapshots. However, the NLOS channel lacks the direct LOS component, resulting in a reduced concentration of power and increased delay dispersion. This complexity poses challenges in differentiating between NLOS and LOS scenarios, particularly when the identification technique relies on simpler models. Higher error rates are caused by the increased complexity of multipath propagation and timing discrepancies, which make accurate identification more difficult in RMS delay spread scenario. In this work, the channel features are categorized into conventional features and angular-based features, with the latter further subdivided into static and time-varying angular features, as illustrated in Table 2.

5.3 Performance analysis based on localization

The proposed method is assessed using various testing and training methods. We create various training sets made up of diverse groupings of features, for instance, to assess the effect of choosing various features on LOS identification. Each set, which possesses the features indicated by the checkmarks, is shown in Table 3. Different sets of features are used for the training.

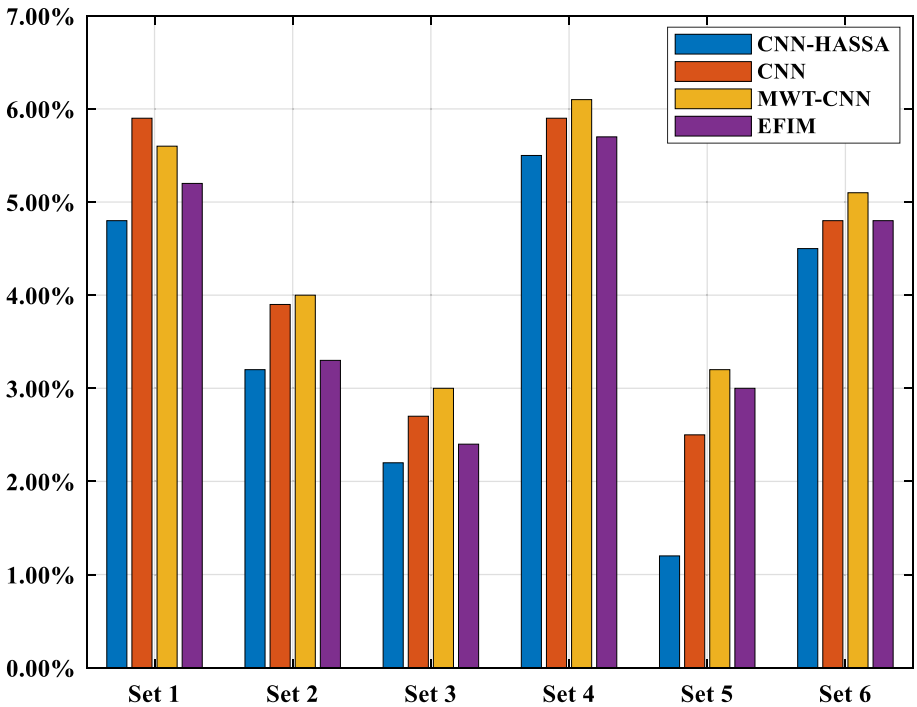

Fig. 8 Identification error rate for different sets

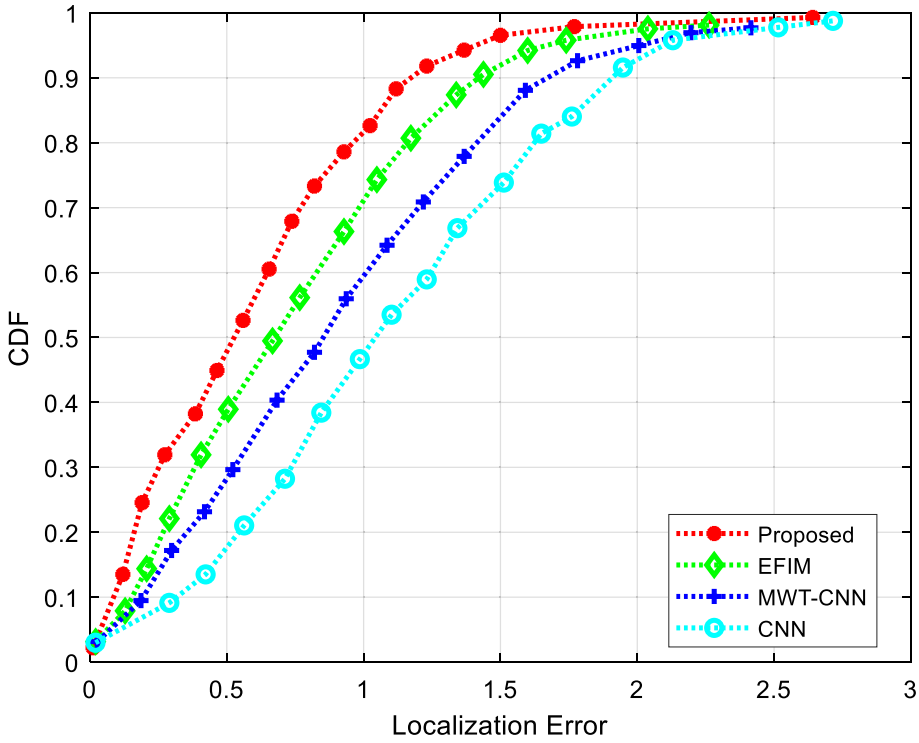

Fig. 9 The CDF versus the average localization error in LOS condition

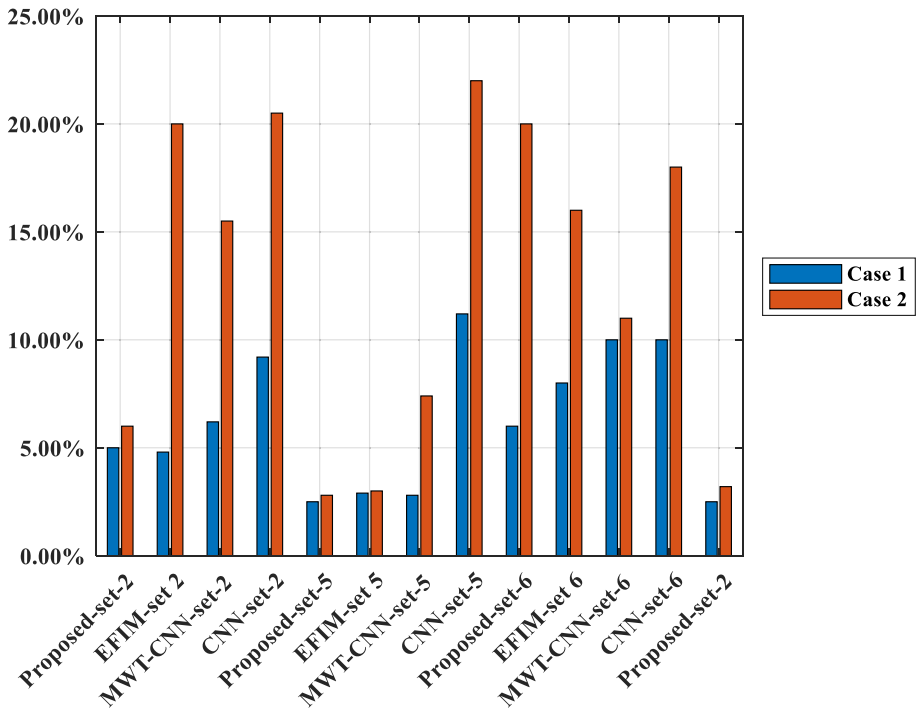

Fig. 10 The effect of data selection on localization error for different identification algorithms with various feature sets

The channel features are separated into conventional features and angular-based features, and the angular-based features are further divided into static and temporal features. This work focuses on examining the statistical and angular properties of MPCs to identify NLOS scenarios. The analysis is centered on eight crucial characteristics: power, skewness, RMS delay spread, kurtosis, rising time, angular departure variation, angular arrival variation, and angular distance. We select these features on the basis of their significant effect on NLOS recognition in our particular circumstance. This selection offers a thorough perspective on channel behavior, prioritizing the most influential

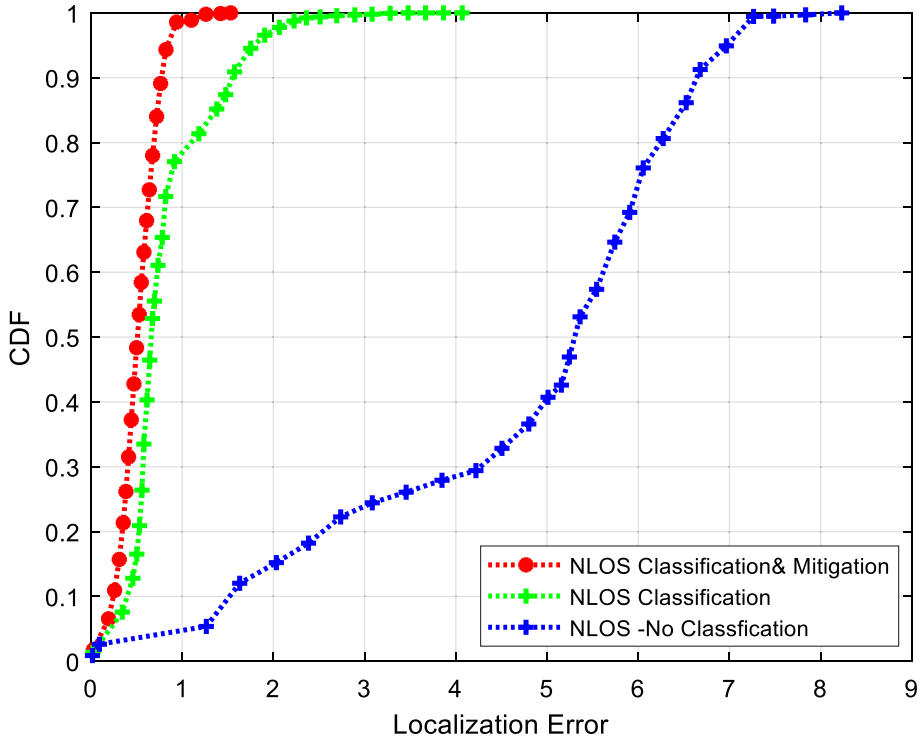

Fig. 11 The impact of mitigation and LOS/NLOS classification on the accuracy of localization in case 1

parameters to provide effective simulations. As a result, this technique provides a clear understanding of how these features influence the outcomes.

5.4 Performance analysis localization based on NLOS/LOS Identification

The state-of-the-art analysis of the identification error rate is depicted in Fig. 8. The EFIM [9], MWT-CNN [11], CNN [12], and proposed CNN-HASSA methods are considered as the state-of-the-art methods to validate the identification error rate. The results confirm that compared with the existing methods, the proposed CNN-HASSA method offers less identification error rate with respect to all the sets described in Table 2.

The location errors before and after NLOS mitigation can be analyzed by examining the cumulative distribution function (CDF) alongside the location error measured in meters. The statistical analysis of error probabilities for four position estimation approaches is illustrated in Fig. 9. Specifically, CNN-SSA, EFIM, MWT-CNN, and CNN exhibit localization errors of 0.8, 1, 1.25, and 1.5 m, respectively, taking into account an estimation error ratio of 0.74. These findings underscore the success of the proposed CNN-SSA-based identification technique in significantly enhancing localization accuracy within massive MIMO systems.

5.5 Performance analysis localization based on NLOS Mitigation

EDDPG-HBA approach relies on NLOS mitigation. The most influential factor impacting identification accuracy is the choice of training characteristics. Figure 10 illustrates the location error before and after the proposed approach to NLOS mitigation. The identification error rate for the various algorithms that were trained using the feature sets is shown in Table 2. This study delves into two distinct cases of training and validation data to scrutinize the impact of data selection on identification accuracy. Case 1 employs K-fold cross-validation, while case 2 utilizes entirely separate sets of data for training and validation. The effect of data selection on identification error rates and localization error has been evaluated for both cases 1 and 2, considering various feature sets in Table 2 as shown in Fig. 10. To provide context, we also compare the performance of our proposed methods in both cases against CNN, EFIM, and MWT-CNN. Upon comparing performance across different datasets, it becomes evident that approaches employing case 1 training procedures consistently yield the highest performance levels. Conversely, methods using Case 2 exhibit lower performance levels.

Figure 10 also demonstrates that angular-based characteristics can enhance the resilience of LOS/NLOS identification, even when validating data varies. Furthermore, the CNN-HSSA-based identification algorithm achieves a commendable level of recognition accuracy, showcasing its potential in diverse scenarios. It observed from Fig. 10 that in both cases, mitigating the NLOS improves the location error. Notably, the CNN-HASSA-based identification exhibits superior performance in both scenarios within Set 5. These findings highlight the CNN-SSA method's enhanced resilience in addressing NLOS identification challenges compared to EFIM, MWT-CNN, and CNN methods utilizing angular features.

Figure 11 illustrates the cumulative distribution functions (CDFs) of NLOS errors both before and after mitigation. In case 1, the probability of errors less than 1 m significantly increases from 78 to 98%. Similarly, the figure also demonstrates the influence of NLOS classification, revealing a substantial rise in the probability of errors smaller than 1 m, escalating from 5 to 78%. This reduction in error is particularly evident, decreasing from nearly 6.7 m to 1.5 m following NLOS identification. The identification and mitigation of NLOS greatly improves the localization accuracy. The CNN-HASSA-based identification method significantly enhances localization processing, outperforming the blind approach, and the application of the EDDPG-HBA technique significantly improves NLOS mitigation.

6 Conclusion

The primary objective of our work was to distinguish between NLOS and LOS conditions within a MIMO system. We achieved this objective by utilizing features extracted from a channel, which were classified as high- and low-resolution parameters derived from the channel impulse response. Using these extracted features, we successfully identified LOS and NLOS scenarios by employing the proposed CNN-HASSA. This approach significantly enhanced the localization accuracy in the MIMO system. As a result, we addressed the identified NLOS conditions by implementing EDDPG-HBA. This method effectively mitigates NLOS scenarios. Our experimental analyses demonstrated a notable reduction in identification error and location error when our proposed approach was employed, which was achieved with minimal computational overhead. Furthermore, the computational complexity of our approach was negligible compared with its substantial performance improvements.

Acknowledgements This work is technically supported by the University of Kent. This work was also funded thanks to the University of Thi-Qar, Ministry of Higher Education and Scientific Research, Iraq.

Author contributions F.G: conceptualization, methodology, formal analysis and investigation, writing—original draft preparation; H.Z: investigation, review, editing and supervision and J.W review and supervision.

Funding This study was funded by University of Thi-Qar, MT-293949.

Data availability The datasets generated during and/or analysed during the current study are available from the corresponding author on reasonable request.

Declarations

Competing interests The authors declare no competing interests.

Open Access This article is licensed under a Creative Commons Attribution-NonCommercial-NoDerivatives 4.0 International License, which permits any non-commercial use, sharing, distribution and reproduction in any medium or format, as long as you give appropriate credit to the original author(s) and the source, provide a link to the Creative Commons licence, and indicate if you modified the licensed material. You do not have permission under this licence to share adapted material derived from this article or parts of it. The images or other third party material in this article are included in the article's Creative Commons licence, unless indicated otherwise in a credit line to the material. If material is not included in the article's Creative Commons licence and your intended use is not permitted by statutory regulation or exceeds the permitted use, you will need to obtain permission directly from the copyright holder. To view a copy of this licence, visit http://creativecommons.org/licenses/by-nc-nd/4.0/.

References

1. Pan C, Ren H, Wang K, Elkashlan M, Nallanathan A, Wang J, Hanzo L. Intelligent reflecting surface aided MIMO Broadcasting for simultaneous wireless information and power transfer. IEEE J Sel Areas Commun. 2020;38(8):1719–34. https://doi.org/10.1109/jsac.2020.3000802.

2. Eichner C, Paquette M, Mildner T, Schlumm T, Pléh K, Samuni L, Crockford C, Wittig RM, Jäger C, Möller HE, et al. Increased sensitivity and signal-to-noise ratio in diffusion-weighted MRI using multi-echo acquisitions. Neuroimage. 2020;221:117172. https://doi.org/10.1016/j.neuroimage.2020.117172.
3. Ahmed AH, Al-Heety AT, Al-Khateeb B, Mohammed AH. Energy efficiency in 5G massive MIMO for mobile wireless network. In: 2020 International Congress on Human-Computer Interaction, Optimization and Robotic Applications (HORA). 2020. https://doi.org/10.1109/hora49412.2020.9152847.
4. Al-Hourani A. On the probability of line-of-sight in urban environments. IEEE Wireless Commun Lett. 2020;9(8):1178–81. https://doi.org/10.1109/lwc.2020.2984497.
5. Zhang P, Yang B, Yi C, Wang H, You X. Measurement-based 5G millimeter-wave propagation characterization in vegetated suburban macrocell environments. IEEE Trans Antennas Propag. 2020;68(7):5556–67. https://doi.org/10.1109/tap.2020.2975365.
6. Liu X, Velten A. The role of wigner distribution function in non-line-of-sight imaging. 2020. https://doi.org/10.1109/iccp48838.2020.9105266.
7. Perovic NS, Di Renzo M, Flanagan MF. Channel capacity optimization using reconfigurable intelligent surfaces in indoor mmWave environments. 2020. https://doi.org/10.1109/icc40277.2020.9148781.
8. Huang C, Molisch AF, He R, Wang R, Tang P, Ai B, Zhong Z. Machine learning-enabled LOS/NLOS identification for MIMO systems in dynamic environments. IEEE Trans Wireless Commun. 2020;19(6):3643–57. https://doi.org/10.1109/twc.2020.2967726.
9. Mendrzik R, Wymeersch H, Bauch G, Abu-Shaban Z. Harnessing NLOS components for position and orientation estimation in 5G millimeter wave MIMO. IEEE Trans Wireless Commun. 2019;18(1):93–107. https://doi.org/10.1109/twc.2018.2877615.
10. Jian M. NLOS OAM-MIMO transmission: misaligned channel analysis and pre-processing scheme design. 2020. https://doi.org/10.1109/iwcmc48107.2020.9148466.
11. Cui Z, Gao Y, Hu J, Tian S, Cheng J. LOS/NLOS identification for indoor UWB positioning based on Morlet wavelet transform and convolutional neural networks. IEEE Commun Lett. 2021;25(3):879–82. https://doi.org/10.1109/lcomm.2020.3039251.
12. Zeng T, Chang Y, Zhang Q, Hu M, Li J. CNN-based LOS/NLOS identification in 3-D massive MIMO systems. IEEE Commun Lett. 2018;22(12):2491–4. https://doi.org/10.1109/lcomm.2018.2872522.
13. Hariq SH, Karakaya B, Odabasioglu N. Outage analysis of MIMO NLOS-UV communication systems over atmospheric turbulence channels. IET Commun. 2020;14(14):2294–302. https://doi.org/10.1049/iet-com.2020.0068.
14. Femenias G, Lassoued N, Riera-Palou F. Access point switch ON/OFF strategies for green cell-free massive MIMO networking. IEEE Access. 2020;8:21788–803. https://doi.org/10.1109/access.2020.2969815.
15. Basit A, Wang W-Q, Nusenu SY. Adaptive transmit array sidelobe control using FDA-MIMO for tracking in joint radar-communications. Digit Signal Process. 2020;97:102619. https://doi.org/10.1016/j.dsp.2019.102619.
16. Garcia-Morales J, Femenias G, Riera-Palou F. Energy-efficient access-point sleep-mode techniques for cell-free mmWave massive MIMO networks with non-uniform spatial traffic density. IEEE Access. 2020;8:137587–605. https://doi.org/10.1109/access.2020.3012199.
17. Sheikh TA, Bora J, Hussain MA. Sum-rate performance of massive MIMO systems in highly scattering channel with semi-orthogonal and random user selection. Radioelectron Commun Syst. 2018;61(12):547–55. https://doi.org/10.3103/s0735272718120026.
18. Bakulin MG, Rejeb TB, Kreyndelin VB, Smirnov AE. Combined precoding technique with antenna selection for massive MU-MIMO systems. In: 2021 Systems of Signals Generating and Processing in the Field of on Board Communications. 2021. https://doi.org/10.1109/ieeeconf51389.2021.9416114.
19. Guvenc I, Chong C-C, Watanabe F. Analysis of a linear least-squares localization technique in LOS and NLOS environments. IEEE Vehicular Technol Conf. 2007. https://doi.org/10.1109/vetecs.2007.391.
20. Chen H, Zhang Y, Li W, Tao X, Zhang P. ConFi: convolutional neural networks based indoor Wi-Fi localization using channel state information. IEEE Access. 2017;5:18066–74. https://doi.org/10.1109/access.2017.2749516.
21. Rizk-Allah RM, Hassanien AE, Elhoseny M, Gunasekaran M. A new binary salp swarm algorithm: development and application for optimization tasks. Neural Comput Appl. 2018;31(5):1641–63. https://doi.org/10.1007/s00521-018-3613-z.
22. Hashim FA, Hussain K, Houssein EH, Mabrouk MS, Al-Atabany W. Archimedes optimization algorithm: a new metaheuristic algorithm for solving optimization problems. Appl Intell. 2020;51(3):1531–51. https://doi.org/10.1007/s10489-020-01893-z.
23. Dhiman G. SSC: a hybrid nature-inspired meta-heuristic optimization algorithm for engineering applications. Knowl-Based Syst. 2021;222:106926. https://doi.org/10.1016/j.knosys.2021.106926.
24. Liu W, Peng L, Cao J, Fu X, Liu Y, Pan Z, Yang J. Ensemble bootstrapped deep deterministic policy gradient for vision-based robotic grasping. IEEE Access. 2021;9:19916–25. https://doi.org/10.1109/access.2021.3049860.
25. Drawil NM, Amar HM, Basir OA. GPS localization accuracy classification: a context-based approach. IEEE Trans Intell Transp Syst. 2013;14(1):262–73. https://doi.org/10.1109/tits.2012.2213815.
26. Hashim FA, Houssein EH, Hussain K, Mabrouk MS, Al-Atabany W. Honey Badger Algorithm: new metaheuristic algorithm for solving optimization problems. Math Comput Simul. 2022;192:84–110. https://doi.org/10.1016/j.matcom.2021.08.013.
27. Chitambira B, Armour S, Wales S, Beach M. NLOS identification and mitigation for geolocation using least-squares support vector machines. 2017. https://doi.org/10.1109/wcnc.2017.7925566.
28. Fu J, Fu Y, Xu D. Application of an adaptive UKF in UWB indoor positioning. 2019. https://doi.org/10.1109/cac48633.2019.8996692.

Publisher's Note Springer Nature remains neutral with regard to jurisdictional claims in published maps and institutional affiliations.